The Mystery of the 41meV Peak in the High-T_c Cuprates

Shashank Misra
University of Illinois- Urbana Champaign
(May 13, 1999)

The discovery by J. Rossad-Mignod *et al.* of a sharp quasiparticle peak in neutron scattering spectroscopy data taken on the High T_c superconductor $YBa_2Cu_3O_7$ at optimal doping has sparked considerable interest in this spectroscopic feature and its effect on superconductivity. [7]. Using neutron scattering spectroscopy, Fong *et al.* conclusively demonstrated that this spectroscopic feature exists only below T_c and is magnetic in nature in optimally doped YBCO. [9] Their technique fascilitated the characterization of this feature with respect to doping, temperature, disorder, and sample type using neutron scattering. [11,12,14,15] Photoemission spectroscopy measures a sudden change in electronic structure, namely the appearance of the peak-dip-hump feature, upon cooling below T_c. [23,24] This feature exhibits similar behavior to the quasiparticle peak as a function of temperature and doping. [25,26] As a result of their similar behaviors, some have conjectured that the 41meV 'mystery' might be responsible for the pairing interaction in High T_c superconductors.

I. INTRODUCTION

Since the discovery of high T_c superconductors by Bednorz and Muller in 1986, the physics of the superconducting state of these materials has remained controversial. These materials, the high T_c cuprates, all share a common perovskite crystal structure containing layers of Cu-O planes perperndicular to the c-axis of the crystal. When it was determined that the parent compounds of the cuprates are antiferromagnetic insulators, in contrast to BCS superconductors which are good metals, many began to think that the physics behind High-T_c superconductivity was fundamentally different. (Fig. 1) Other differences in their properties from a traditional BCS description were soon discovered: a highly anisotropic gap (compared to the isotropic BCS gap function), a ratio of $\frac{2\Delta_{max}}{T_c} \approx 3 - 11$ (compared to the BCS result of 3.5) [21], the existence of a gap above T_c [2], and the existence of a sharp quasiparticle peak at 40meV binding energy [7]. Some of the most powerful tools in characterizing these properties are spectroscopic, as these directly measure the quantum states of the system. Among them, research using two techniques in particular has been vigorous- neutron scattering spectroscopy and photoemission spectroscopy. Two cuprate materials in particular have attracted a lot of attention- $YBa_2Cu_3O_{7-x}$ (YBCO) and $Ba_2Sr_2CaCu_2O_{8+x}$ (BSCCO).

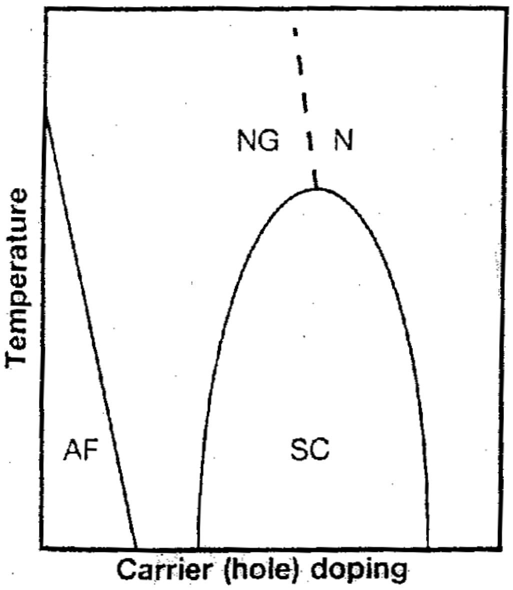

FIG. 1. A sketch of the phase diagram for the cuprate superconducting compounds. Here, AF stands for antiferromagnetic insulator, SC stands for superconductor, NG stands for gapped normal state (metallic), and N stands for normal state (metallic). [1]

The sharp quasiparticle peak located at 41 meV binding energy in optimally doped YBCO, along with the opening of the superconducting gap below T_c and the abrupt change in the low energy electronic states of the system below T_c, are the three spectroscopic signatures of the superconducting state of the cuprates. Being one of the hallmark features of superconductivity, many scientists believe that the 41meV peak contains information about the nature of the interaction that pairs electrons into Cooper pairs. This article reviews the experimental investigations of the 41meV quasiparticle peak in the High T_c cuprates using neutron scattering spectroscopy, along with a handful of photoemission spectroscopy experiments on the electronic states of these systems that suggest that the 41meV peak is related to the sudden change in electronic properties of the cuprates at T_c.

II. NEUTRON SCATTERING SPECTROSCOPY

A. Experimental Details

Neutron scattering spectroscopy (NSS) has been a very useful tool in investigating the quasiparticle peak in the superconducting cuprates, as it not only detects magnetic and vibrational states as a function of both energy and momentum, but it is also sensitive to the polarization of the states it measures.

A ballistic, single-particle picture serves to illustrate the basic principles behind NSS experiments. A beam of neutrons with known energy and momentum is incident on a sample, and the reflected beam's momentum and energy is measured. Energy conservation gives $\Delta E = E_f - E_i$; conservation of crystal momentum gives $\Delta \mathbf{k} = \frac{1}{\hbar}\mathbf{p_f} - \frac{1}{\hbar}\mathbf{p_i} + \mathbf{G}$, where $\mathbf{G}$ is a reciprocal lattice vector. $\Delta E(\Delta \mathbf{k})$ is the energy (wavevector) transferred from the sample to the neutron. The main complication of NSS is that many physical processes might be reponsible for a peak in the scattering cross section as a function of ΔE and $\Delta \mathbf{k}$. In the case of $\Delta E = 0$, the initial and final states of the sample are identical, and the wavevector restriction is simply Bragg's law. Accordingly, this case simply gives the Bragg peaks of the crystal lattice. Next, consider the case where ΔE and $\Delta \mathbf{k}$ correspond to a single excitation of the system (e.g. absorbing a single phonon or magnon). For a given excitation (e.g. the acoustic phonon branch), we now have $E_a(\frac{1}{\hbar}(\mathbf{p_f} - \mathbf{p_i})) = \frac{\mathbf{p_f}^2}{2m} - \frac{\mathbf{p_i}^2}{2m}$ where I have assumed that E_a is periodic in reciprocal lattice vectors. This condition will be satisfied in (functionally) different ways for different excitations of the system. Peaks in the scattering cross section as a function of ΔE and $\Delta \mathbf{k}$ will map out the E and $\mathbf{k}$ dependence of states of the system. Finally, consider the case where ΔE and $\Delta \mathbf{k}$ correspond to multiple excitations of the system. Even in the simplest such case of scattering off of two acoustic phonons, momentum conservation and energy conservation do not lead to a well-determined equation (i.e., they result in relationships of several $E_a(\mathbf{k_a})$'s that can be satisfied for a range of values of ΔE and $\Delta \mathbf{k}$). These terms lead to a broad background in the scattered intensity. [3]

NSS is used to not only measure spectral features, but also the magnetic (or non-magnetic) nature of these features. A polarized neutron scattering system is pictured in Fig. 2. A collimated beam from a neutron source enters the apparatus at the left. It passes first through a crystal M that serves as both a monochromator (and a polarizer, depending on choice of crystal) of the incoming neutron beam. The device R, when turned on, adiabatically flips the spin of the incoming beam. The sample is mounted in a chamber located in an electromagnet F that exerts minimal field on the sample, but ample enough field on the incident and scattered neutron beam to rotate its polarization to lie in the direction of the field. That is, this field can be used to rotate the direction of polarization of the neutrons to some fixed angle away from some quantization axis of the sample. The three G devices serve as guide fields. The first serves to keep the neutrons polarized in the same direction after they leave the monachromator and before entering the flipper R. The second and third ones are nearly mirror images of one another- they change the axis of polarization of the neutrons from being aligned with the monachromator to being at a desired angle with respect the field produced by the electromagnet F (second), and from some desired angle with respoect to the field produced by F to being aligned with the analyzer A (third). In this way, the experimenter has complete control over the angle of polarization of the neutrons with respect to the scattering vector of a state, the angle of polarization the analyzer will detect for, and any tendency of the scattering potential to flip the spins of the neutrons (i.e. if there is a spectral peak while the flipper is on, but none when it is off). [4] Different geometrical configurations of the analyzer crystal A and the counter C select for different energy and momenta transfers (and, by choice of crystal, polarization). NSS data is presented as either the scattered intensity or the imaginary part of the dynamical susceptibility $Im(\chi)$ (explained in the next paragraph) as a function of $\mathbf{k}$, using the units of reciprocal lattice units (rlu; i.e. k_x is in units of $\frac{2\pi}{a}$, etc.), and energy.

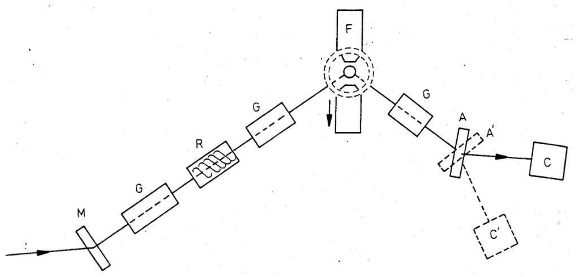

FIG. 2. An idealized schematic diagram of a polarization sensitive neutron scattering spectrometer. Letters represent the main components of this device, and are referred to in the text (from Kiebeck and Brown [4]).

As alluded to by the layout of the spectrometer, the precise description of the process of NSS is much more complicated than the simple single-particle one presented earlier. A more thorough derrivation yields that the scattering cross section is directly proportional to the dynamical structure factor of a crystal. [5] The dynamical structure factor, in turn is propotional to the imaginary part of the dynamical susceptibility, $\chi((\mathbf{K}, \hbar\omega)$, multiplied by a Bose function after removal of any contributions from phonons. Starting from Fermi's Golden Rule, the inelastic scattering cross section can be expressed as

$$\frac{d\sigma}{d\Omega dE} \propto \sum_{\alpha\beta}(\delta_{\alpha\beta} - \mathbf{k}_\alpha \mathbf{k}_\beta) S_{\alpha\beta}(\mathbf{k}, E), \tag{1}$$

where

$$S_{\alpha\beta}(\mathbf{k}, E) \propto \sum_R e^{i\mathbf{k}\cdot\mathbf{R}} \left| \int dE \frac{d^3\mathbf{r}}{V} \langle \Phi_f | V(\mathbf{R}) | \Phi_i \rangle \right|^2$$

$$\propto \frac{Im(\chi(\mathbf{k},\hbar\omega))}{1-exp(\hbar\omega/kT)}, \tag{2}$$

In these equations, α and β refer to spin polarizations, Φ_i and Φ_f denote the many-body wave functions of the sample before and after the scattering, and $V(\mathbf{r})$ is the scattering potential. Thus, the data are roughly proportional to the dynamical structure factor $S_{\alpha\beta}(\mathbf{k},E)$, the Fourier transform of the scattering potential of a system as a function of energy and momentum.

There are many complications in interpreting neutron scattering data. [6] First of all, these experiments measure very low intensities. Thus the intensity of a spectrum is usually increased at the cost of energy resolution whenever possible. The relatively low intensities involved in these experiments also limits investigators to using very large samples; until recently, this has limited them to looking at only YBCO single crystals. Second, the nature of the losses of beam intensity in various parts of the aparatus can be difficult to identify and quantify. This makes any analysis of absolute intensities difficult. Lastly, this technique measures both the vibrational and magnetic excitations of the system. In experiments using unpolarized spectrometry, the proper identification of the vibrational contribution to the spectra is crucial. As these features are subtracted from the cross section before converting the cross section into $Im(\chi)$ (as most data is presented), artifacts in the shape of $Im(\chi)$ can result. Even in experiments where it is possible to measure spin-flip and non-spin-flip cross sections, the low scattered intensities involved coupled with the imprecision of the equipment can produce spectral artifacts. For these reasons, this report concentrates only on only general characteristics of the quasiparticle peak, and not on a precise analysis of the spectral lineshape.

B. Experimental Results

Early NSS studies of the superconductung cuprates concentrated on characterizing spectral features below energy transfers of 25meV on heavily underdoped samples, ones very close to the transition from superconductor to antiferromagnetic insulator in the cuprate phase diagram. The NSS investigation of the 41 meV peak began in 1991 when J. Rossad-Mignod *et al.* demonstrated the ability to resolve magnetic features of neutron scattering spectra above 25meV. [7] Their experiment used an unpolarized spectrometer (similar to Fig. 2, except without the flipper) and nearly optimally doped YBCO single crystals with $T_c = 92K$. Fig. 3 shows $Im(\chi)$ as a function of energy taken at $\mathbf{k} = (0.5, 0.5, 5.2)$ rlu for the indicated temperatures. Elastic and suspected vibrational contributions to the scattering cross section were first subtacted from the raw data to convert it into $Im(\chi)$. At T=5k, a quasiparticle peak is clearly visible at 41meV; by T=81K, quasiparticle feature has broadened significantly and moved to lower energy. Once T crosses T_c, the integrated intensity of the spectra falls dramatically, indicating that this feature is related to the phenomena of superconductivity. Spectra taken at T=5K measuring intensity versus q in $\mathbf{k} = (q, q, 5.2)$ rlu) for various energy shifts are shown in Fig. 4. For E=40meV, the spectrum shows that the quasiparticle feature is located roughly at q=0.5, with another much sharper feature located at q=0.8 (this second feature was later identified as a 43meV phonon mode). While the selection of $\mathbf{k} = (0.5, 0.5, 5.2)$ rlu prevents contamination by this phonon mode, the complicated analysis employed in this report obviated the need to perform polarization sensitive measurements.

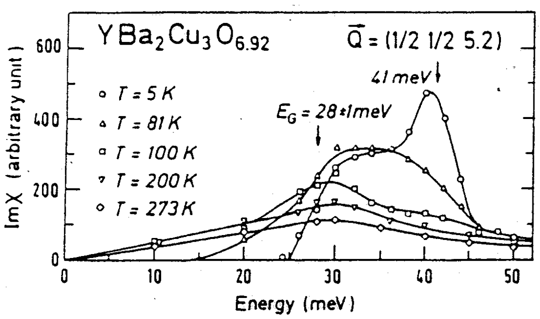

FIG. 3. $Im(\chi)$ as a function of energy for $\mathbf{k} = (1/2, 1/2, 5.2)$ taken on a YBCO sample of T_c=91K. Data taken at T=5K is plotted using circles; data taken at T=81K is plotted using upward pointing triangles. Disregard other plots. [7]

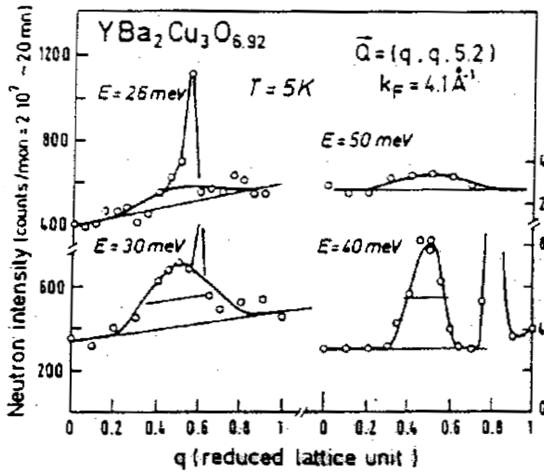

FIG. 4. Scattering intensity as a function of H at E=40meV and $\mathbf{k} = (H, H, 5.2)$ is plotted in the lower right panel. Data was taken at T=5K on the same sample as Fig. 3. Disregard other plots. [7]

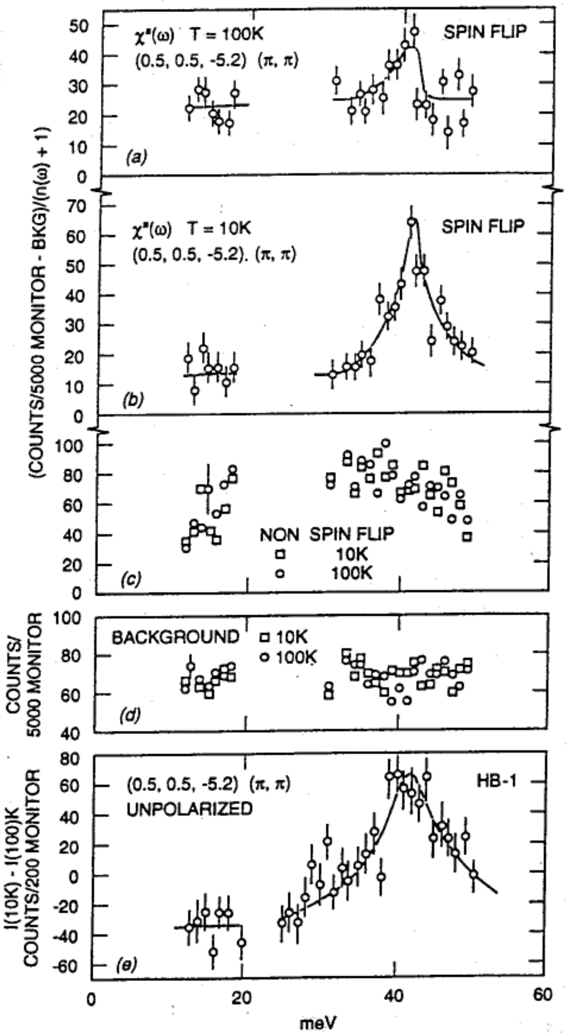

FIG. 5. Polarization sensitive spectra for $\mathbf{k} = (0.5, 0.5, 5.2)$ fixed. (a,b) The spin-flip contribution to $Im(\chi)$ as a function of energy at the indicated temperatures. (c) The non spin-flip contribution to $Im(\chi)$ at the indicated temperatures. (d) The background contribution due to stray counts by the neutron counter, as explained in the text. Data is absolute intensity as a function of energy for the temperatures indicated. (e) An unpolarized measurement of the 100K intensity subtracted from the 10K intensity, as a function of energy. [8]

Two years later, Mook *et al.* successfully performed similar measurements using a device similar to the one shown in Fig. 2. [8] Their experiment focused on taking both non spin-flip (i.e. the spin state of the neutron beam before and after the scattering are the same) and spin-flip measurements in both the superconducting and normal states. This allowed them to seperate the vibrational and magnetic contributions to the quasiparticle peak, as the vibrational contribution should not flip the spin of the scattered neutrons while the magnetic contributions should. The data pictured in Fig. 5 show their results for $Im(\chi)$ versus E=25-50meV for $\mathbf{k} = (0.5, 0.5, -5.2)$ in a nearly optimally doped YBCO cingle crystal ($T_c = 92K$). The region near 25meV was removed because a Bragg reflection at this energy was found to be too intense to filter out. The background was assumed to be the contribution to the scattering cross section with the analyzer crystal pointed away from the counter. This was justified based on the spectra being similar for the sample in both the superconducting (T=10K) and normal states (T=100K). The non-spin flip contribution to the 41meV quasiparticle peak is essentially featureless and remains identical for the both the normal and superconducting state spectra. The quasiparticle peak is clearly visible in the spin-flip spectra, although it is seen both for both normal and superconducting state spectra. The authors concluded that the 41meV peak was magnetic in origin, and that it persisted above T_c. They added that it does not shift in energy as T is increased, but it does decrease in amplitude. The T=100K findings of J. Rossad-Mignod *et al.* that the peak shifts to 25meV as T approaches T_c are contaminated by improper removal of the 25meV Bragg peak and the diminished intensity of the 41meV feature at increased temperatures. The persistence of the peak above T_c was later explained by Fong *et al.* to arise from a small fraction of unflipped neutrons leaking through the flipper and subsequently Bragg reflecting off of nuclei in the sample. [9] Finally, the authors hypthesized that $I(T < T_c) - I(T > T_c)$ for unpolarized NSS might give an accurate portrayal of the quasiparticle feature, as this would subtract out the (featureless) non-magnetic contributions to the intensity.

The persistence of the 41meV peak above T_c motivated a report by Fong *et al.* to prove that this spectral feature was purely magnetic in nature, and that it appeared solely below T_c. [9] Reasoning that the peak seen in spin-flip scattering above T_c might be due to the creation of quasiparticle excitations from the beam of polarized neutrons, and not from already occupied states of the sample, Fong *et al.* devised a clever technique for looking for magnetic features in unpolarized NSS. Specifically, they asserted that the phonon scattering cross section is proportional to the vibrational structure factor:

$$\frac{d\sigma}{d\Omega} \propto \frac{dE}{\omega(\mathbf{k})} \left(\sum_{\mathbf{d}} e^{-i\mathbf{k}\cdot\mathbf{d}} \frac{[\mathbf{K}\cdot \eta_{\mathbf{d}}(\mathbf{k})] e^{-W_{\mathbf{d}}(\mathbf{K})} b_{\mathbf{d}}}{\sqrt{M_{\mathbf{d}}}} \right)^2, \quad (3)$$

where $\mathbf{K}$ is the momentum transferred to the neutron; $\mathbf{k}$ is $\mathbf{K}$ to within an additive reciprocal lattice vector; and $b_{\mathbf{d}}$, $M_{\mathbf{d}}$, and $\eta_{\mathbf{d}}(\mathbf{k})$ are the scattering length, mass and displacement of an atom in the unit cell basis. The authors further noted that the scattering cross section for magnetic scattering events is proportional to the magnetic structure factor:

$$\frac{d\sigma}{d\Omega} \propto \frac{dE}{\omega(\mathbf{k})} f^2(\mathbf{K}) sin^2(\pi L z), \quad (4)$$

where f is the magnetic form factor for the atomic species responsible for the magnetic interaction(Cu), L is the c-axis component of $\mathbf{Q}$, and z is the shortest normalized distance between said atoms. [10,12] A measurement of unpolarized scattering intensity versus L for E=41meV and $\mathbf{k} = (1/2, 1/2, L)$ from an optimally doped YBCO sample is shown in Fig. 6. Notably, while there is a sinusoidal modulation of the intensity, there is also an increase in peak intensity with increased L. Both the above model calculations could lead to this sinusoidal dependance, but only the phonon cross section has increasing intensity with increasing L. Thus they concluded that the 43meV phonon mode, combined with poor energy resolution, could easily account for the increasing intensity as a function of L.

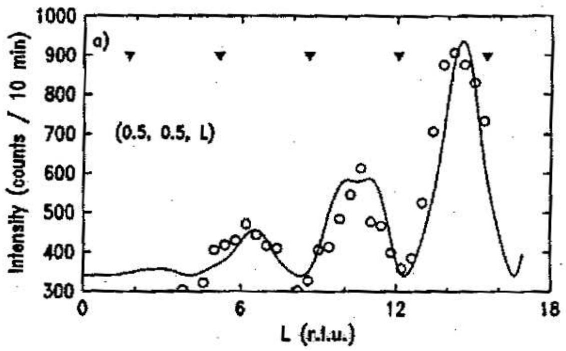

FIG. 6. Scattering intensity as a function of L for E=41meV and $\mathbf{k} = (1/2, 1/2, L)$ is plotted with open circles. Data was taken for T=100K on a YBCO sample with $T_c = 93K$. [9]

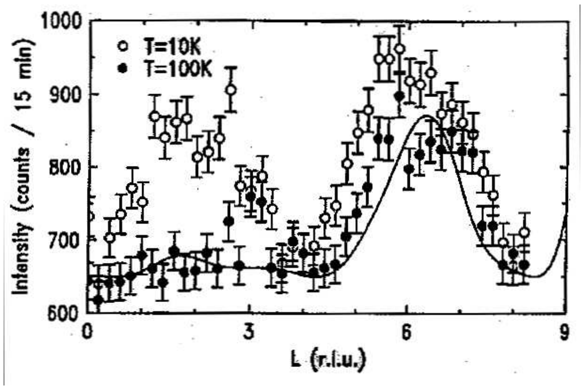

FIG. 7. Scattering intensity as a function of L for E=41meV and $\mathbf{k} = (3/2, 1/2, L)$. Spectra were taken at the indicated temperature on the same sample as Fig. 6 [9]

To confirm their conjecture, Fong *et al.* decided to scan along $\mathbf{k} = (3/2, 1/2, L)$, a reciprocal lattice direction equivalent to the (1/2, 1/2, L) rlu direction, to investigate the scattering cross section for smaller L values. Fig. 7 plots intensity versus L taken on the same sample both in the normal and superconducting state at E=41meV. Two peaks are discernable at T=10K- one centered at L=1.7 and another centered near L=6.2. Another scan taken for T=100K reveals that only the L=6.2 peak remains visible in the normal state; i.e., the structure factor supresses the phonon contribution to the cross section for L=1.7. As final confirmation of their result, a set of scans was taken of intensity versus H with E=41meV and $\mathbf{k} = (3H, H, 1.7)$rlu at T=10K and T=100K. (Fig. 8, top) The momentum width of the 41meV peak is seen to be resolution limited (i.e. the measured momentum width of the peak is roughly equivalent to the resolution of the spectrometer) and therefore seems unusually narrow, c.f. compared to the momentum widths of phonon peaks [7] or spin-wave peaks [10]. Since the normal state spectra (intensity versus energy, not shown) are featureless for $\mathbf{k} = (3/2, 1/2, 1.7)$, Mook's suggestion that $I(T) - I(T > T_c)$ gave an accurate picture of the characteristics of this magnetic state is valid. The bottom left plot of Fig. 8 measures the difference of the scattered intensities at T=10K and T=100K as a function of energy for $\mathbf{k} = (3/2, 1/2, -1.7)$. The data indicate that the energy width of the quasiparticle peak is unusally narrow as well, since it is resolution limited as well. This report conclusively demonstrated that the 41meV quasiparticle peak is magnetic in nature and exists only in the superconducting state. More importantly, it identified a NSS technique to reliably characterize it.

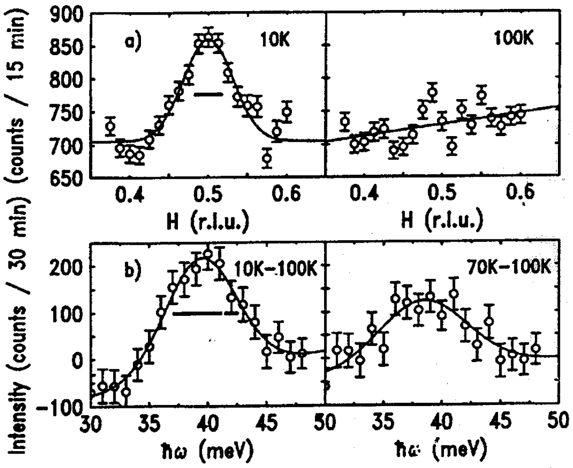

FIG. 8. All data were taken on the same sample as in Fig. 6 (a) Scattering intensity as a function of H for E=41meV and $\mathbf{k} = (3H, H, 1.7)$ taken at the indicated temperatures. The momentum resolution of the spectrometer is indicated by the horizontal bar. (b, left panel) The difference of the scattering intensities at T=10K and T=100K as a function of energy for $\mathbf{k} = (3/2, 1/2, 1.7)$ fixed. The energy resolution of the spectrometer is shown as the horizontal bar. [9]

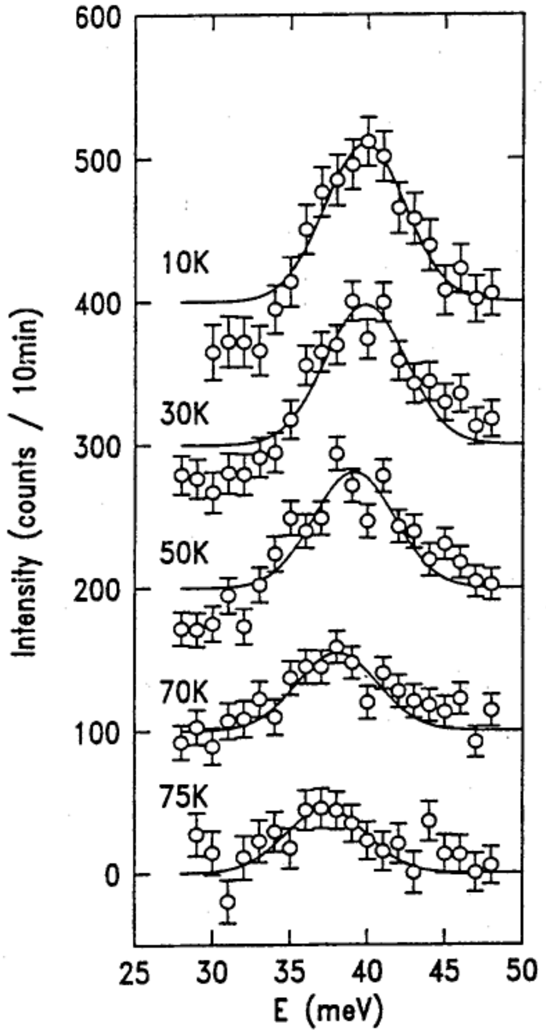

FIG. 9. Scattering intensity as a function of energy for various temperatures with the T=100K intensity subtracted from the spectra. Data is for a YBCO single crystal of $T_c = 93K$ for $\mathbf{k} = (3/2, 1/2, -1.7)$ fixed. The lines are fits to a Gaussian lineshape. Note that the broadening of the peak is attributable to thermal broadening. [11]

Shortly thereafter, several studies seeked to characterize the quasiparticle peak's dependence on temperature and doping, the state variables that specify which portion of the phase diagram a superconductor is in. Fong *et al.* proceeded to determine the temperature dependance of this state using unpolarized NSS. [11] Fixing $\mathbf{k} = (3/2, 1/2, 1.7)$, they looked at $I(T) - I(T = 100K)$ for optimally doped YBCO (see Fig. 9). As a function of increasing temperature, the quasiparticle peak shifts to slightly lower energy, and the integrated intensity of the feature decreases to zero at T_c. (Fig. 10)

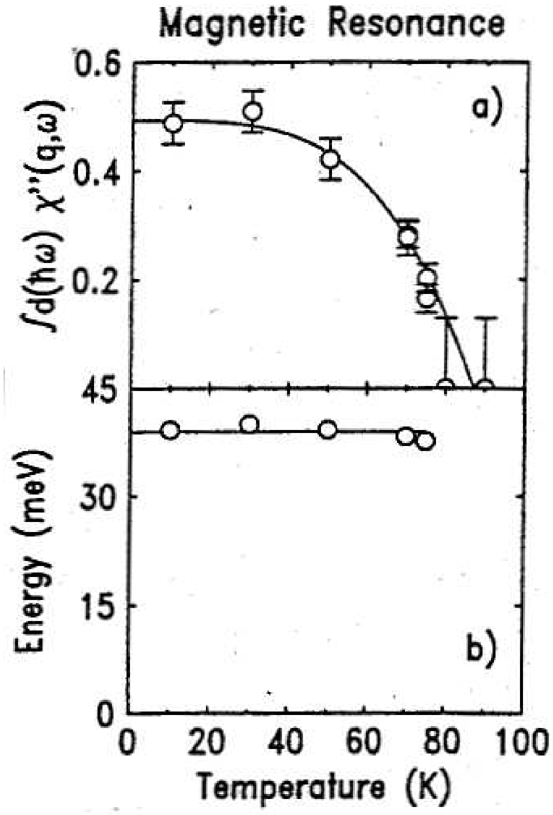

FIG. 10. Integrated intensity (a) and energy location (b) of fits to the quasiparticle peaks in Fig. 9 as function of temperture. The lines through the data are there to serve as guides to the eye. Note in particular the mean field-like dependance of (a). [11]

The doping dependence of the quasiparticle peak was first studied using this method by P. Dai *et al.*. [12,13] Taking a YBCO sample underdoped to $T_c = 62K$, they performed a polarized neutron study for $\mathbf{k} = (-3/2, -1/2, 1.7)$. Fig. 11 indicates that: one, the non spin-flip intensities are identical in both the normal and superconducting state; two, the spin flip $Im(\chi)$ has a quasiparticle peak in the superconducting state at E=35meV, with a weak feature persisting above T_c. The latter prompted the authors to look at intensity for E=35meV and $\mathbf{k} = (3/2, 1/2, 1.7)$ fixed as a function of temperature. The data in Fig. 12 for both spin-flip polarized and unpolarized intensity exhibit the same curious behaviour- the quasiparticle intensity shows the expected behaviour for $T < T_c$, but it continues to decrease above T_c. This contrasts to the flat temperature dependence above T_c observed in optimally doped YBCO. [8]. This feature, even above T_c is verifyably magnetic in nature, as evidenced by the identical temperature dependence of the intensity in both the unpolarized and the spin-flip spectra. The authors suggested that this might indicate persistence of the quasiparticle feature above T_c, but the low intensities involved necessitated further investigation. A similar study by Fong *et al.* did verify this result, and also showed that the intensity increases dramatically at the onset of superconductivity. [12] Data on highly underdoped ($T_c = 52K$) samples reported in the same paper verified that the quasiparticle peak energy decreases monotonically with decreased doping. They further added that the 43meV phonon peak in optimally doped YBCO remains at 43meV in all underdoped samples studied; i.e., it is not coupled to the quasiparticle peak.

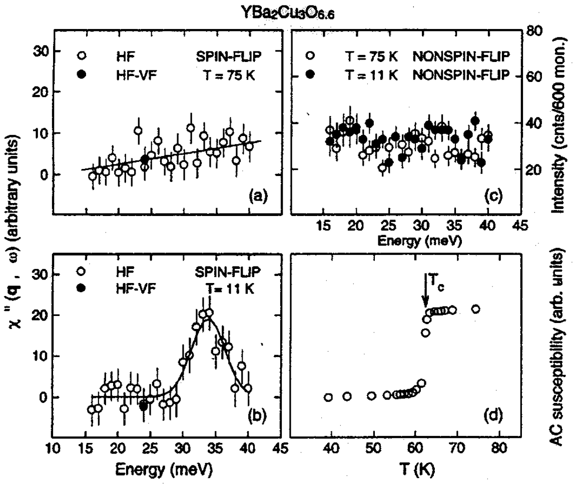

FIG. 11. Polarization sensitive data for an underdoped YBCO sample with $T_c = 63K$ at $\mathbf{k} = (-1/2, -3/2, 1.7)$ fixed. (a) The spin-flip contribution to $Im(\chi)$ as a function of energy at T=75K. (b) The same quantity for T=11K. (c) The non spin-flip scattering intensity for T=75K (open circles) and T=11K (filled circles). (P. Dai *et al.*, [12])

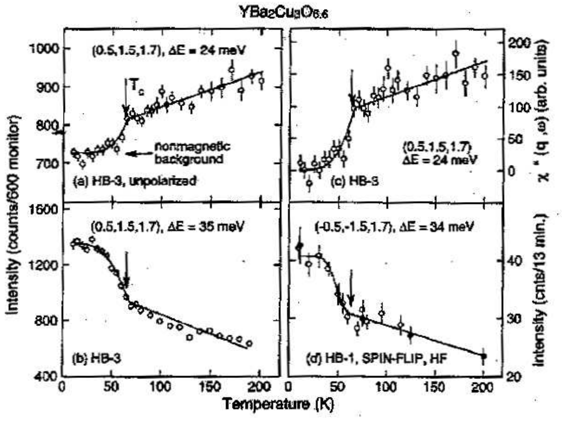

FIG. 12. All data are for the same sample used in Fig. 11 for E=35meV and $\mathbf{k} = (1/2, 3/2, 1.7)$ fixed. (b) Scattering intensity as a function of temperature. (d) The spin-flip contribution to $Im(\chi)$ as a function of temperature. Disregard panels (a) and (c). [12]

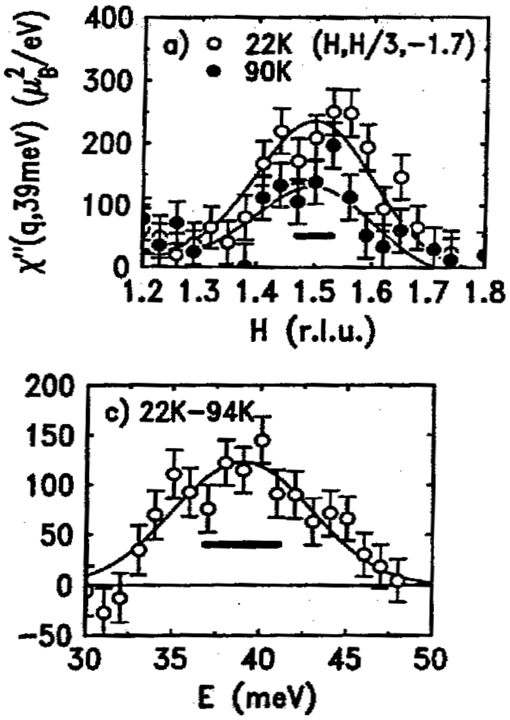

FIG. 13. All data are taken from a YBCO sample with 5 percent substitution of Zn for Cu and maximum oxygen concentration ($T_c = 87K$). (a) $Im(\chi)$ as a function of H for $\mathbf{k} = (H, H/3, -1.7)$ and E=39meV taken at T=22K (open circles) and T=90K (closed circles). The momentum resolution of the spectrometer is indicated by the thick solid line. (c) $Im(\chi)$ as a function of energy for $\mathbf{k} = (1.5, 0.5, -1.7)$ taken by subtracting the T=94K data from the T=22K data. The energy resolution of the spectrometer is shown as the thick solid line. [14]

Fong and collaborators have recently published two key reports that examine the behavior of the quasiparticle peak in cuprate systems significantly different from doped YBCO. The first report focuses on the effects of nonmagnetic impurities in YBCO. [14] The crystal studied was grown with Zn atoms substituted for one in every two hundred Cu atoms, and wad subsequently fully oxygenated ($T_c = 87K$). Zn atoms have been shown to substitute for Cu atoms in the Cu-O planes, introducing minimal structural disorder. While they do not substantially alter the doping level of YBCO, they do introduce magnetic disorder in the Cu-O planes by inducing magnetic moments on neighboring Cu atoms. (as alluded to earlier, the Cu in the Cu-O planes are associated with the magnetic excitations [10]). Lastly, Zn substitution is known to rapidly suppress superconductivity in YBCO (all these results are referenced in [14]). The rapid reduction of T_c with introduction of magnetic disorder in the Cu-O planes suggests that magnetic interactions play a key role in the superconducting mechanism. Since such a small Zn substitution does not significantly alter the phonon spectrum, the experiment could be conducted in a fashion identical to that described earlier. The top panel of Fig. 13 shows normalized $Im(\chi)$ data versus H for E=39meV and $\mathbf{k} = (H, H/3, -1.7)$. Peaks in the spectra centered at H=1.5 occur on data taken both above and below T_c. The bottom panel shows $Im(\chi(T = 22K)) - Im(\chi(T = 90K)$ versus energy taken for $\mathbf{k} = (1.5, 0.5, -1.7)$. The data show a well-resolved peak at 39meV; this shift is most likely due to the small reduction in T_c from optimal doping in this sample. While the quasiparticle peak is centered at the expected values of $\mathbf{k}$ and E, both the momentum and energy widths of the feature are significantly larger than the widths for optimally doped samples. This is attributed to the magnetic disorder induced in the Cu-O planes by the Zn substitution. D ata for $Im(\chi)$ as a function of temperature for E=39meV and $\mathbf{k} = (1.5, 0.5, -1.7)$ fixed is shown in Fig. 14. The quasiparticle feature clearly extends far above T_c. It also has a markedly different shape than the data for both optimally doped and underdoped samples- there is no sharp increase in the peak intensity upon crossing below T_c.

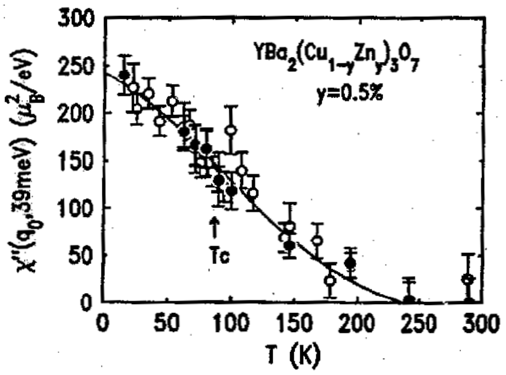

FIG. 14. $Im(\chi)$ as a function of temperature for E=39meV and $\mathbf{k} = (3/2, 1/2, -1.7)$. All data was taken on the same sample as Fig. 13. [14]

The second paper by Fong *et al.* is the first report of NSS spectra taken on BSCCO single crystals. Since NSS data relies on the coherent superposition of scattered waves from layers of the sample, and BSCCO forms crystals in thin plates, it had been very difficult to get a sample large enough to produce satisfactory counting statistics. The authors managed to grow a large enough optimally doped BSCCO single crystal ($T_c = 91K$) to take NSS data. Reasoning that BSCCO and YBCO have reasonably similar properties, they simply looked for the quasiparticle peak near E=40meV and $\mathbf{k} = (0.5, 0.5, L)$, being careful to check for anamolous background features. L=-14 was chosen to give maximum intensity in the spectra. Figure 15 is a plot of intensity versus H for E=43meV and $\mathbf{k} = (H, H, -14)$ for both the normal and superconducting states of the sample. The quasiparticle peak is visible only in the superconducting state, centered around H=0.5. A plot of $I(T = 10K) - I(T = 100K)$ versus E for $\mathbf{k} = (0.5, 0.5, -14)$ clearly shows the peak centered at E=43meV (Fig. 16). Lastly, they measured intensity as a function of temperature for E=43meV and $\mathbf{k} = (0.5, 0.5, -14)$ fixed (Fig. 17). The expected behavior is once again seen- the quasiparticle feature loses intensity as the temperature increases towards T_c, vanishing above T_c. While these data provide an excellent comparison with optimally doped YBCO data, showing the two to be very similar, the peak was not unambiguously determined to be magnetic in nature. Despite the use of optimally doped BSCCO, the peak is manifestly not resolution limited in E or $\mathbf{k}$. The result is of considerable value given that most NSS studies have focused on studying YBCO, and most photoemission spectroscopy investigations have focused on BSCCO.

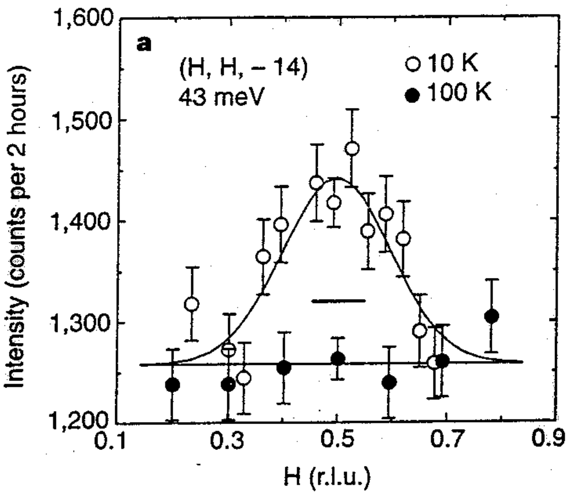

FIG. 15. Scattering intensity as a function of H for E=43meV and $\mathbf{k} = (H, H, -14)$. Data taken from the optimally-doped BSCCO sample ($T_c = 91K$) is plotted at T=10K (open circles) and T=100K (closed circles). The heavy solid line indicates the energy resolution of the spectrometer. Notably, the peak is not resolution limited. [15]

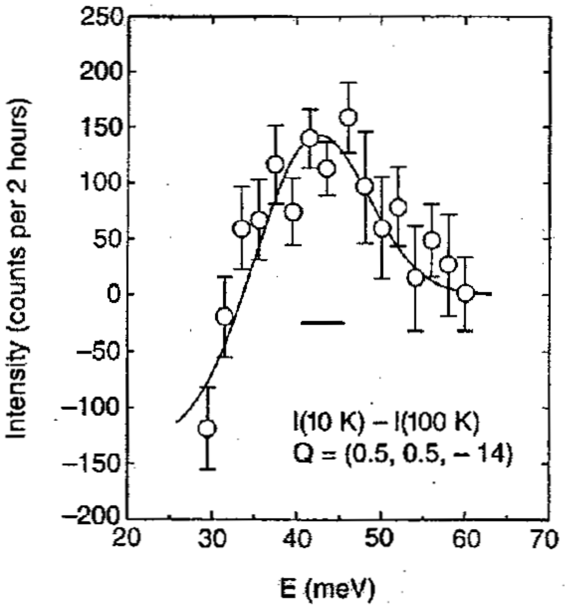

FIG. 16. A measurement of the intensity at T=100K subtracted from the intensity at T=10K as a function of energy for $\mathbf{k} = (1/2, 1/2, -14)$ fixed. The energy resolution of the analyzer is shown with the dark solid line. Note that the peak is not resolution limited. The data was taken from the same sample as Fig. 15. [15]

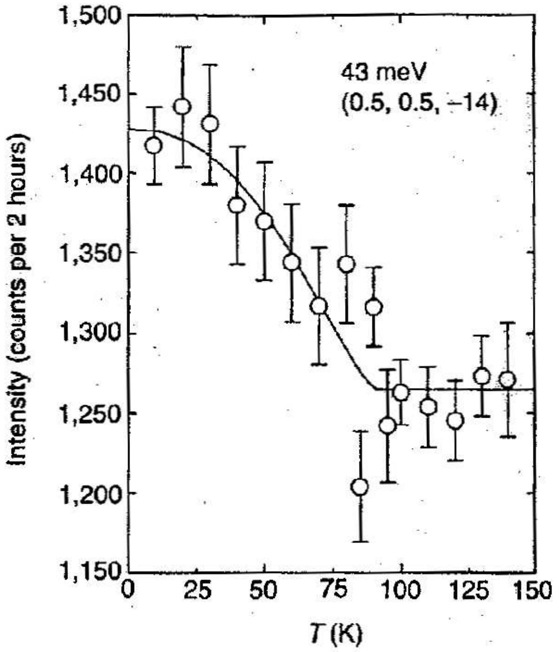

FIG. 17. Scattering intensity as a function of temperature for E=43meV and $\mathbf{k} = (1/2, 1/2, -14)$ fixed. The data was taken from the same sample as Fig. 15. [15]

III. PHOTOEMISSION SPECTROSCOPY

A. Experimental Details

Photoemission spectroscopy has been used extensively to study superconductivity because it also gives a resolved picture of electronic states as a function of both particle energy and momentum. Most photoemission experiments study BSCCO samples because they cleave very cleanly in vacuum, exposing an uncontaminated surface ideal for this surface sensitive measurement.

The basis of photoemission spectroscopy is the photoelectric effect- a photon incident on a material can be absorbed by an electron which, if the incident photon has sufficiently high energy, escapes the material with a characteristic kinetic energy. In ARPES experiments, the incident photon is provided by a high intensity beam of monochromatic photons held at $E = h\nu$ focused on a macroscopic area of the sample. A single electron absorbes a photon, conserving energy in the reaction. Due to translation invariance in the plane parallel to the sample surface, wavevector is conserved along these directions. Typical photon energies are of order 10eV, meaning that typical photon wavenumbers are on the order of 10^{-3}Å^{-1}. Because typical electron wavenumbers are of order 1Å^{-1}, the photon wavevector can be neglected in conserving wavevector parallel to the sample surface. This means that $k_{\|,i} = k_{\|,f}$ within an additive reciprocal lattice vector. Many of the High-T_c compounds (e.g. BSCCO) are layered compounds with very weak interlayer coupling, such that electronic states are thought to have negligible dependance on the perpendicular component of $\mathbf{k}$. As illustrated in Fig. 18, this means that measuring the energy and momentum of the emitted electron gives complete information about its energy and wavevector in the material. Since photoemission is unable to distinguish the k_z dependance of an electronic state, all momenta will be quoted as in-plane momenta $\mathbf{k} = (k_x, k_y)$ in units of rlu. The energy of electrons that escape the sample is measured using an electrostatic electron energy analyzer. This analyzer has an entrance aperture that can be positioned at various angles to the sample; i.e. the analyzer can be positioned to accept only electrons emitted to a specific solid angle. Knowing both the magnitude of electron momentum and the angle of emission precisely determines the wavevector of the emitted electron. By varying both the energy of the incoming photon and the position of the nose cone, it is possiible to map the spectral function (in this naive picture, roughly corresponding to the occupied single electron states in the system) as a function of electron energy and momentum in the sample. [16] A broad background is thought to come from electrons which get scattered before entering the analyzer. Photoemission spectra are usually presented as intensity as a function of binding energy for a fixed value of $\mathbf{k}$. These spectra essentially measure the electronic states of the system.

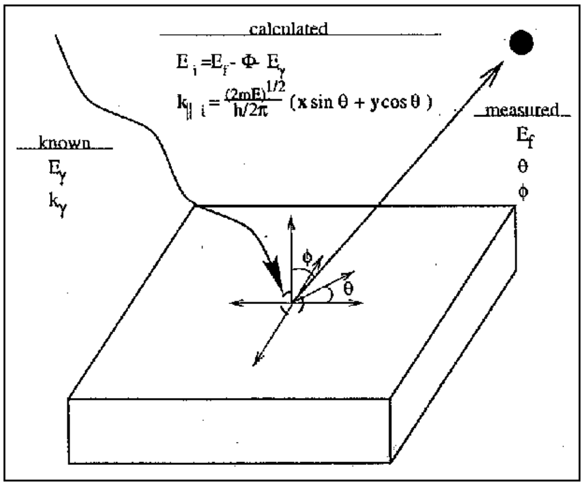

FIG. 18. Idealized layout of a typical photoemission experiment. A photon of known polarization, energy and momentum is pictured coming in from the left. The electron energy analyzer (not pictured) measures the kinetic energy of the ejected electron, shown leaving to the right, if the electron travels into the solid angle of acceptance of the analyzer (fixed ϕ and θ). As shown in the figure, the initial energy and $\mathbf{k}_{\parallel,i}$ can then be calculated. Here Φ gives the work function of the material, usually determined from thermionic emission. The photohole left behind in the process is shown as an empty sphere in the material.

Photoemission is inherently a quantum mechanical phenomenon, and it is useful to think of it using time-dependent perturbation theory. From Fermi's Golden Rule-

$$I \propto A(\mathbf{k}, E)\, |\langle \Phi_f \,|\, \mathbf{A}\cdot\mathbf{p} \,|\, \Phi_i \rangle|^2 \,, \qquad (5)$$

where Φ_i and Φ_f are the initial and final states of the system and A($\mathbf{k}$, E) is the spectral intensity (described in the next paragraph). A polarizing optical element can be placed in the path of the incident beam of photons, allowing experimentalists to set the polarization vector of the photons to point in specific directions in k space. This allows ARPES studies to be sensitive to the polarization dependence of an electronic state through the matrix element in the above expression. However, photoemission is not sensitive to the spin of the ejected electron. While the polarization of an electronic state can be inferred from careful analysis of the dependence of photoemission intensity on photon polarization, this method is not straightforward, as is the case with NSS. For unpolarized incident photons, the matrix element is often approximated as being unity.

While this simple picture captures the essence of photoemission, it overlooks many subtleties. First of all, photoemission is a many-body phenomenon. Formally, photoemission spectroscopy is a quantum statistical problem measuring the three current correlation function. [17] A significant simplification assumes that photoemission is a single-particle process (i.e. considering photoemission one event at a time). Using the so-called sudden approximation, photoemission intensity is given by the time-dependant perturbation theory result. The spectral intensity of an emitted electron, under this approximation, is simply the imaginary part of the single particle Green's function multiplied by a Fermi-Dirac distribution. [6,18] If not for final-state effects (described later), ARPES would measure the single-particle density of states as a function of energy and momentum modulo the Fermi function and the matrix element. Second, the photoemission lineshape is affected by the final state of the system. Both the ejected electron and the screened photohole left behind can result in artifacts in the observed lineshape compared to the expected spectral lineshape of the sample. [19] Lastly, photoemission gives a single-electron picture of the electronic states of a sample. For instance, it doesn't measure Cooper pairs of a superconductor, but rather how Cooper pairs would look mapped onto single-electron picture; i.e., photoemission measures the energy and momentum of an electron that came from first breaking up a Cooper pair, then ejecting the electron from the material. For these reasons, while ARPES may seem to measure the density of single-particle electronic states of the system, the observed lineshapes are often deceiving and difficult to interpret. [20] With this cautionary note, the location of spectral features in $(E, \mathbf{k})$ space and their dependance on state variables such as sample temperature and doping can reveal important electronic characteristics of a system without resorting to theoretical models.

B. Experimental Results

Even though C. Olson *et al.* first observed a sharp quasiparticle feature in the electronic states of the superconducting state of BSCCO using ARPES [21], seven years passed before anyone attempted to look specifically at this feature. [22] H. Ding *et al.* first investigated the quasiparticle peak in nearly optimally doped BSCCO single crystals ($T_c = 87K$). [23] Figure 19 shows the measured photoemission intensity as a function of electron energy at T=13K and $\mathbf{k} = (1, 0)$. Not only is a sharp quasiparticle feature seen near E=30meV, but a dip near E=70meV and a hump near E=100meV are also clearly resolved. Both the peak and dip are resolution limited in E. Ding *et al.* next attempted to show that this peak and the higher energy hump and dip are part of the same feature. By varying the incident photon angle with respect to the z-axis of the sample, the dipole matrix element $\langle \mathbf{A}\cdot\mathbf{p} \rangle$ also changes. If the peak, dip and hump are part of the same feature, the intensities of all three should show the same dependance on incident photon angle because of the photoemission matrix element. As can be seen in Fig. 19, spectra taken for incident angle 15^o and 85^o, when rescaled to have the same intensity in the quasiparticle peak, are identical in shape. If the three features were unrelated, the dip and hump features would differ significantly in the two sets after the quasiparticle peak intensities are made to match. The authors concluded that a higher binding energy dip and hump feature are intimately related to this sharp peak.

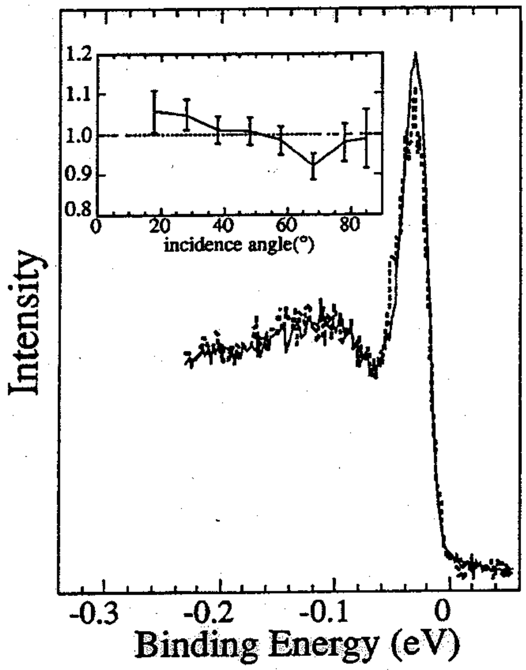

FIG. 19. Photoemission intensity versus binding energy taken at $\mathbf{k} = (1, 0)$ and T=13K from an optimally doped BSCCO single crystal ($T_c = 87K$). The solid line is taken for a photon incidence angle of 18^o from the sample surface normal direction, and the dashed line is taken for a photon incidence angle of 85^o. The sharp peak feature is resolution limited. [23]

Another report by the same group showed a set of high-resolution spectra taken on a BSCCO sample- one spectra for the normal state of the sample, one for the superconducting state. [24] The data were taken on a sample with the same T_c and at the same point in $\mathbf{k}$ space. The intensity versus energy data shown in Fig. 20 show four major features of these spectra: one, the superconducting gap is present only in the superconducting state spectrum; two, the sharp quasiparticle peak is present only in the superconducting state spectrum; three, the higher binding energy dip is present only in the superconducting state spectrum; and four, the two spectra begin to share the same energy dependence at even higher binding energies. The peak-dip-hump feature thus seems to be, along with the superconducting gap, intimately tied with superconductivity in BSCCO.

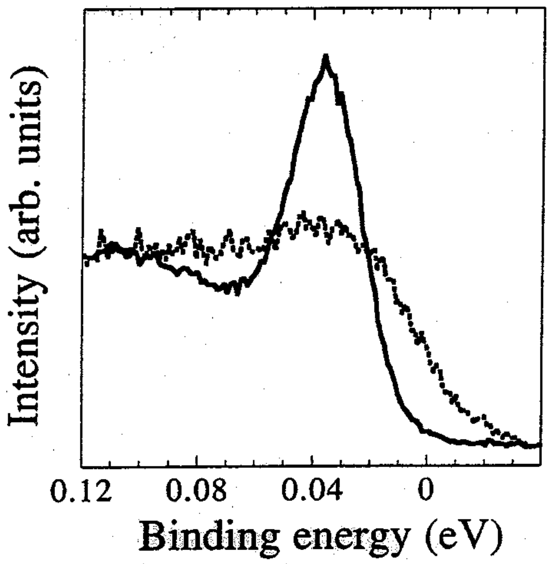

FIG. 20. Photoemission intensity versus binding energy taken at T=105K (dotted line) and T=13K (solid line) from a BSCCO single crystal of T_c=87K. The data were taken at the $\mathbf{k} = (1, 0)$ point. [24]

Although such studies are far from complete, investigators have begun looking at the temperature and doping dependance of the peak-dip-hump feature using ARPES. A.G. Loeser *et al.* have taken high resolution photoemission spectra of the peak-dip-hump structure at non-optimal doping. [25] Their data, shown in Fig. 21 looks at photoemission intensity at the $\mathbf{k} = (1, 0)$ point as a function of energy for two samples- one overdoped BSCCO crystal ($T_c = 86K$, bold line) and another underdoped BSCCO crystal ($T_c = 79K$, dotted line). These spectra show the decrease in spectral intensity of the sharp peak with decreased doping level. In addition, they also show that the intensity undergoes an overall decrease at energies less than the hump energy, remaining roughly the same for energies greater than the energy. While enough high resolution data is not currently available, these data suggest that the peak-dip-hump feature loses intensity with decreased doping. Recently, A.V. Federov *et al.* published a fairly thorough investigation of the temperature dependence of this feature. [26] They took high-resolution photoemission spectroscopy data on optimally doped BSCCO at various temperatures for $\mathbf{k} = (1, 0)$. Subsequently, the extracted two parameters from these spectra: the intesnity of the sharp peak, and the binding energy of the leading edge of the hump (which they call Δ_o). These parameters are plotted as a function of temperature in Fig. 22. The Δ_o parameter shows an almost mean field-like decrease in energy as T increases. While the intensity of the sharp peak shows similar behavior approaching T_c from below, it persists above T_c. This behaviour has also been noted before in underdoped BSCCO, and led some to believe that the dip-hump may be directly tied with superconductivity, but that the sharp peak may not. [27] The general tendencies of both the peak-dip-hump feature in ARPES measurements and the quasiparticle peak in NSS measurements are very similar- both have reduced intensity with decreased doping levels, and both decrease in magnitude in a roughly mean-field-like fashion with increasing temperature.

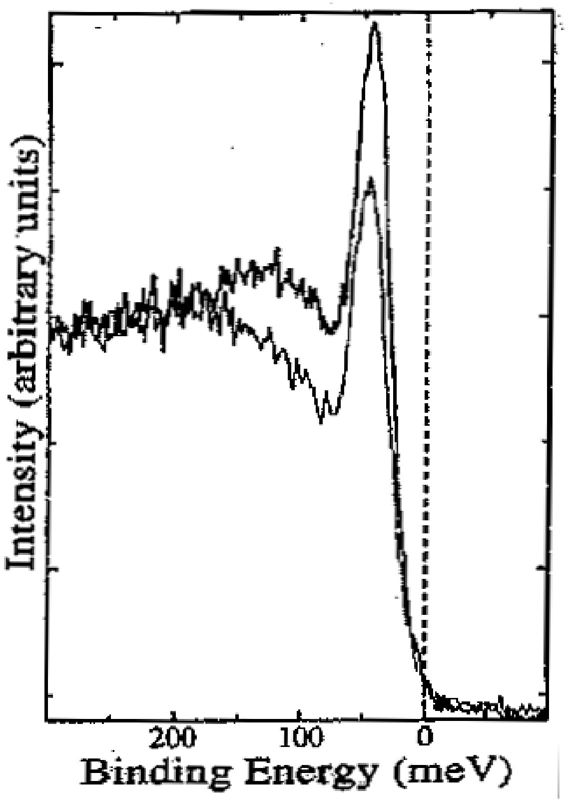

FIG. 21. Photoemission intensity as a function of binding energy taken at the $\mathbf{k} = (0, 1)$ point in the superconducting state for a slightly overdoped BSCCO sample of $T_c = 86K$ (solid line) and a slightly underdoped BSCCO sample of $T_c = 79K$ (dashed line). [25]

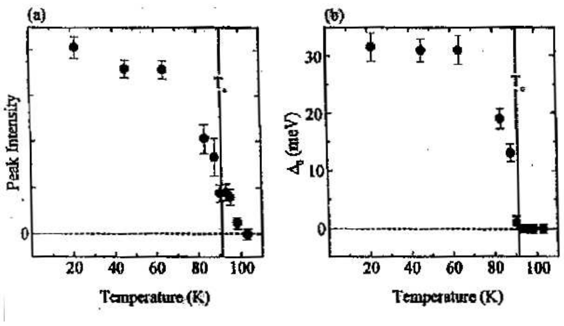

FIG. 22. All data are were taken on an optimally doped BSCCO single crystal ($T_c = 91K$) at the $\mathbf{k} = (1, 0)$ point. (a) Intensity of the sharp peak feature versus temperature. (b) The energy location of the low-binding energy side of the hump feature as a function of temperature. [26]

Based on the shape of the Fermi surface in optimally doped BSCCO as measured with ARPES, Z.-X. Shen and Robert Schrieffer have proposed that the 41meV quasiparticle might be responsible for the electronic features seen by ARPES. [27] While their analysis is beyond the scope of the report, the motivation for suggesting this possibility is easily understood. The quasiparticle peak (NSS) and the peak-dip-hump feature (ARPES) have both been shown to appear near the superconducting transition, (seperately) exhibit features (e.g. narrowness of both peak features) suggestive of collective behavior, and share similar temperature and doping dependance. The rapid suppression of T_c with the introduction of magnetic disorder lends credence to the suggestion that the 41meV peak, a magnetic state showing signs of being a collective state, is strongly coupled to the electronic states of the superconducting state. The Fermi surface of optimally doped BSCCO is shown in Fig. 23 in units of π rlu. Notice that the Fermi surface extends to the Brillouin zone boundary only near along the $\langle 0, \pi \rangle$ and $\langle \pi, 0 \rangle$ directions. This is where nearly all the high resolution ARPES data has been taken becuase it is along these directions that the most substantial variation in spectral intensity is seen with respect to state variables (like doping and temperature). An excitation associated with momentum transfer (π, π) (e.g. the 41meV quasiparticle) would serve to connect these spots on the Fermi surface, while not being able to link any others.

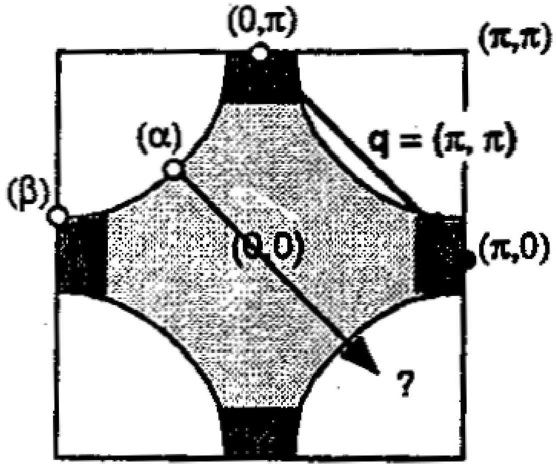

FIG. 23. The Fermi surface of the superconducting state of optimally doped BSCCO has been mapped using ARPES. A simplified version of the Fermi surface is shown as the shaded area. Here, reciprocal lattice distances are quoted in units of π rlu. Notice that electronic features such as those located at β could be connected to other similar points on the fermi surface by a quasiparticle with $\mathbf{k}$=(π, π), but points such as α could not. [27]

IV. CONCLUSION

Determination of whether or not the 41meV quasiparticle peak is responsible for pairing will require further investigation. NSS work on BSCCO crystals is necessary to see how the results compare with ARPES data. ARPES data on overdoped BSCCO is substantially different from the data taken in the underdoped regime. Just as importantly, experiments could study the behaviour of the 41meV quasiparticle peak in the overdoped part of the phase diagram. Second, full characterization of the peak-dip-hump feature in ARPES would serve to solidify some of the conjectured parallels between its behaviour and the quasiparticle peak's behaviour. Lastly, the temperature dependence of both these features, namely their tendency to persist above T_c, is a seperate mystery in and of itself. Many suggest that this may be the signature of incoherent superconducting pairs forming above T_c.

---

[1] A.G. Loeser *et al.*, Science **273**, 325 (1996).
[2] B.G. Levi, Physics Today, June 1996, 17 and references therein.
[3] N. Ashcroft, and D. Mermin, **Solid State Physics**, Harcourt Brace College Publishers, Orlando: 1976, pp. 470-480.
[4] R.M. Moon, T. Riste, and W.C. Koehler, Phys. Rev. **181**, 920 (1969). K.R.A. Kiebeck and P.J. Brown, J. Phys. F **10**, 2015 (1980).
[5] Roughly from N. Ashcroft, and D. Mermin, **Solid State Physics**, Harcourt Brace College Publishers, Orlando: 1976, 780. For more details, see M. Kastner *et al.*, Rev. Mod. Phys. **70**, 896 (1998) and references included therein.
[6] Many-body effects in the sample can have a dramatic effect on the spectum in all these techniques. In a system with weak interactions, a Fermi liquid, this doesn't introduce any serious complications because particle and quasiparticle states of the sample will still correspond to peaks in the spectra with known lineshapes. However, in the strongly interacting limit, i.e. in a non-Fermi liquid, the system is dominated by collective effects and doesn't have quasiparticles. While peaks in the spectral intensity do still correspond to characteristic features of this collective state, they are not to be interpreted as quasiparticle states. For example, many theorists believe that the normal state of underdoped cuprates is indeed a non-Fermi liquid. While this is an extreme example, it should be remembered that complex many-body effects are present and do make the analysis of lineshapes model-dependant.
[7] J. Rossad-Mignod *et al.*, Physica C **185-189**, 86 (1991).
[8] H.A. Mook *et al.*, PRL **70**, 3490 (1993).
[9] H.F. Fong *et al.*, PRL **75**, 316 (1995).
[10] That the Cu in the Cu-O planes were intimately tied with the magnetic interactions in YBCO has been investigated using NSS. See, e.g.
J.M. Tranquada *et al.*, PRB **40**, 4503 (1989).
[11] H.F. Fong *et al.*, PRB **54**, 6708 (1996).
[12] P. Dai *et al.*, PRL **77**, 5425 (1996);
H.F. Fong *et al.*, PRL **78**, 713 (1997).
[13] $YBa_2Cu_3O_{7-x}$ is optimally doped for x=0, and becomes underdoped for x¿0. There is no overdoped phase.
[14] H.F. Fong *et al.*, PRL **82**, 1939 (1999).
[15] H.F. Fong *et al.*, Nature **398**, 588 (1999).
[16] For a more complete discussion see
N.V. Smith, "Angular Dependant Photoemission" in Cordona, M. and Ley, L., **Photoemission in Solids I**, Springer-Verlag, New York: 1978, pp. 237-264.
[17] Conceptually, the formal derrivation considers photoemission to be a three step process: 1. the sample initially at equilibrium not in presence of a radiation field; 2. application of the radiation field; 3. the sample at equilibrium in the radiation field. The strict theoretical formalism is presented in
W.L. Schaich, "Theory of Photoemission" in Cordona, M. and Ley, L., **Photoemission in Solids I**, Springer-Verlag, New York: 1978,pp.l05-134 and references therein (I could not make sense of it).
[18] M. Franz and A. J. Millis, PRB **58**, 14572 (1998) and references therein.
[19] The technique is measuring characteristics of the propogation of an electron escaping the material (hence, conceptually why the intensity is proportional to the imaginary part of the single particle Green's function), which will be influenced by the final state of the system. These effects can be quite dramatic. For example, R. Joynt has proposed that the psuedogap seen in the quasi one dimensional conductors, the minganates, and possibly even the cuprates might be due to the electric field of the ejected electron (R. Joynt, Science **284**, 777 (1999)).
[20] For a discussion of the impact of some many-body effects on ARPES studies of the normal state Fermi surface and the superconducting gap see
Z.X. Shen *et al.*, Science **267**, 343 (1995).
[21] C.G. Olson *et al.*, Science **245**, 731 (1989).
[22] I am not referring to the same quaiparticle peak when discussing photoemission data as I was earlier when discussing the NSS data. Both quasiparticle peaks happen to be sharp. However, not only do they have different characteristics, one is measured using magnetic spectroscopy (NSS) and the other in electronic spectroscopy (ARPES).
[23] H. Ding *et al.*, PRL **76**, 1533 (1996).
[24] M.R. Norman *et al.*, PRL **79**, 3506 (1997).
[25] A.G. Loeser *et al.*, PRB **56**, 14185 (1997).
[26] A.V. Federov *et al.*, PRL **82**, 2179 (1999).
[27] Z.-X. Shen and J.R. Schrieffer, PRL **78**, 1771 (1997).